Differences in urban heat island and its driving factors between central and new urban areas of Wuhan, China

Manuscript submitted to ***Environmental Science and Pollution Research***

Differences in urban heat island and its driving factors between central and new urban areas of Wuhan, China

Xie Chen[1], Shicong Zhang[2], Zhiyong Tian[1,*], Yongqiang Luo[1], Jie Deng[3], Jianhua Fan[4]

[1] School of Environmental Science and Engineering, Huazhong University of Science and Technology, Wuhan, China, 430074

[2] Institute of Building Environment and Energy, China Academy of Building Research, Beijing 100013, China

[3] School of Computing and Engineering, University of West London, St Mary's Road, Ealing, London, W5 5RF, UK

[4] Department of Civil Engineering, Technical University of Denmark, Brovej 118, 2800 Kgs. Lyngby, Denmark

*Corresponding author: zhiyongtian@hust.edu.cn (Z. Tian)

Abstract

Urban heat island (UHI) is one of the important effects of urbanization on built environment. Land surface temperature data was taken from moderate-resolution imaging spectroradiometer (MODIS) to investigate the long-term spatiotemporal patterns of UHI in Wuhan during 2001~2018 and, the UHI intensity changes of built-up land in 13 administrative regions in Wuhan were analyzed. Furthermore, 34 spatial error models and 34 ordinary least squares models were established and compared. Spatial error models showed good fitting effect, which were used to determine the influence of normalized difference vegetation index (NDVI), normalized difference building index (NDBI), and social–economic factors (population and nighttime light) on UHI intensity in central urban area and new urban area. The explanatory power changes of these four indicators during 2001~2018 were explored as well. The average UHI intensity in 2014~2018 has increased by about 0.45 ℃ compared to that in 2001~2005. NDBI is the most dominant factor contributing to the increase in temperature. The impact of NDVI on UHI intensity changes from negative to positive, and the impact of NDBI on UHI intensity in central urban area is weakened during 2001–2018. Social–economic factors have a greater impact on new urban area than on central urban area. These findings show the effects and the explanatory power changes of driving factors during 18 years, which can provide a better understanding of the formation and development of UHI and support for the future urban planning of Wuhan.

Keywords: Urban heat island; Land surface temperature; Spatial autocorrelation; Spatial error model

Differences in urban heat island and its driving factors between central and new urban areas of Wuhan, China

Introduction

With the rapid process of industrialization and globalization, the level of urbanization in China has continued to rise. Since reform and opening up, China has changed a lot in a very short period of time, and a large number of rural people have poured into cities, achieving a leap in urbanization (Zhang 2008). According to the seventh national census, the level of urbanization has continued to increase. The urban population reaches 901.99 million, accounting for 63.89%, and the rural population is 509.79 million, accounting for 36.11%. Compared to 2010, the proportion of urban population increases by 14.21% in 2020. It is estimated that in 2030, 1 billion Chinese people will live in urban areas (Taylor 2015). Rapid urbanization has brought many achievements, providing residents with safer housing conditions, better quality of education, and better medical treatment. But there are also many problems and adverse effects. The development of urbanization will lead to the loss of wildlife habitats, destroying biodiversity (Hughes 2017); result in environment pollution (Hao et al. 2020); and cause eutrophication of water bodies (Jiang et al. 2008). At the same time, urbanization destroys the surface energy balance and brings the urban heat island (UHI) (Monteiro et al. 2021). UHI is one of the main adverse effects of urbanization. It is a phenomenon that the temperature in urban area is higher than that in the suburb. UHI will affect the urban ecological environment, causing local temperatures to rise, thereby increasing the demand for refrigeration and increasing energy consumption (Yang et al. 2020). UHI will also have a secondary impact on the weather, bringing more thunderstorms (van Heerwaarden and de Arellano 2008). Human life and health will be threatened by high temperature, aggravating cardiovascular diseases and respiratory diseases, thus leading to heatstroke and even death (Macintyre and Heaviside 2019). There are two categories of UHI, atmospheric urban heat island (AUHI) and surface urban heat island (SUHI). AUHI can further be divided into boundary layer UHI and canopy layer UHI. Boundary layer UHI refers to the air temperature difference between urban and rural areas in the layer from rooftop or treetop to the atmosphere unaffected by urban landscapes. Towers and radiosondes are used for the air temperature measurement. However, different temperature sensors make it difficult to do the temperature

comparison, and climate model simulation is usually used to describe boundary layer UHI (Hu et al. 2019). Canopy layer UHI refers to the air temperature difference between urban and rural areas in the layer from surface to rooftop or treetop. It mainly uses the data from ground observations or automobile transects (Pichierri et al. 2012). SUHI mainly relies on remote sensing satellite data to retrieve land surface temperature (LST). After 2005, studies on SUHI have increased exponentially, because the interest of UHI increases and the quantity and quality of remote sensing data have been enhanced (Zhou et al. 2018). Satellite remote sensing data can better perform the spatiotemporal patterns of temperature compared to data from ground observations or automobile transects, which gives a full sight to the urban thermal environment of Wuhan. Therefore, SUHI using the remote sensing data is focused. The formation and development of UHI is affected by many factors. The process of urbanization has led to the conversion of a large number of natural surfaces into impervious surfaces. The impervious surfaces absorb heat during the day and release it slowly at night, changing the balance of surface energy, causing temperature rise and leading to UHI (Morabito et al. 2016). In addition, the increase of impervious surface will accelerate the loss of surface water (Haase and Nuissl 2007) and thus affect the local climate. Land cover changes will have an impact on the local climate (Grigoraș and Urițescu 2019). With the advancement of remote sensing technology, some indices based on remote sensing data is widely used in the analysis of driving factors of UHI. The normalized difference vegetation index (NDVI), normalized difference building index (NDBI), and normalized difference water index (NDWI) can identify vegetation, construction land, and water bodies and are proved to have close relationships with LST. NDVI has a negative correlation with LST (Karakuş 2019). Because the transpiration of vegetation (Boegh et al. 1999) and moist soil conditions (Carlson et al. 1994; Goward et al. 2002). NDWI reflects the area of water body and also shows a negative correlation with LST (Guha et al. 2019). NDBI has a positive impact on LST (Pathak et al. 2021), and its influence is greater than NDVI and NDWI (Feng et al. 2019). Additionally, social–economic factors like population density and nighttime light also have effects on UHI. It is found that there is a significant positive relationship between population density and LST (Li et al. 2012). The more the population counts, the denser the buildings. Population density and impervious cover are highly correlated in Canadian urban areas, and the LST of heavily populated urban areas is higher (Zhang and Sun 2019). Nighttime light data is widely used to study the process of urbanization (Ma et al. 2012; Yi et al. 2014) and also can be used to predict GDP (Liu et al. 2021a), which means

that nighttime light data can reflect the socio-economic level. It is positively related to impervious surface areas and energy consumption, leading to UHI (Sun et al. 2020). A number of studies have discussed the impact of multiple factors on UHI in China. Yue et al. performed stepwise multiple linear regression to investigate the relationship between UHI and landscape metrics (Yue et al. 2019). Liu et al. analyzed the relationship between UHI and urban form metric at national and regional levels by ordinary least squares regression (Liu et al. 2021b). Li et al. investigated the impact of socioeconomic drivers on annual, summer, and winter average UHI by generalized additive model in major Chinese cities (Li et al. 2020). Yang et al. conducted correlation analysis between the footprint of UHI and associated factors using Spearman's correlation analysis in 302 Chinese cities (Yang et al. 2019). Huang and Wang investigated the relationship between urban morphology and LST using stepwise multivariate linear regression in Wuhan (Huang and Wang 2019). Pearson correlation coefficient and multiple linear regression analysis are often used for the discussion of the driving factors of UHI (Bottyán and Unger 2003; Wang et al. 2020). According to the first law of geography, everything is related to each other; the closer the distance, the stronger the connection (Tobler 1970). Heat will be transferred through conduction, convection, and radiation (Kim et al. 2016). The above methods cannot discuss the spatial relationship of LST. Therefore, the spatial regression models have been proposed. Spatial lag model (SLM) and spatial error model (SEM) are commonly used spatial regression models. And it is found that the fitting effect of SEM is better than ordinary least squares model (OLS) and SLM (Yin et al. 2018; Guo et al. 2020a, b). Several studies have been conducted to analyze the driving factors of UHI in Wuhan using spatial regression models (Lu et al. 2021a, b; Shi et al. 2022). However, the above-mentioned researches use the results of a single year or a single season to investigate the driving factors Environmental Science and Pollution Research 1 3 of UHI. UHI will change dynamically with urban sprawl, and its driving factors will also change. The UHI intensity of cities with different development levels is studied and find that the impact of population on UHI intensity may be stronger in the early stages of urbanization (Cui et al. 2016). The influence of the largest water patch index on UHI in Wuhan has been weakened during 2000~2019, and the influence of the average patch size of forest land has increased by using ordinary least squares models (Wang et al. 2020). The analysis of a single year cannot fully understand the explanatory power changes of driving factors. At present, there are few studies focus on the long-term series of multiple driving factors of UHI while using SEMs. Discussing the influence

changes of each driving factor in the process of urban development will deepen the understanding of the formation and development of UHI and provide better suggestions to alleviate UHI, thus helping the healthy development of the city. Therefore, it will be important to fill the gap in long-term series analysis of the explanatory power changes of driving factors using SEMs. Wuhan is chosen as the study area. It is known as the 'Stove Cities' in China and is one of the nine national central cities in China, playing an important role in politics, economy, and culture. The urbanization rate in Wuhan has increased from 40.59% in 2001 to 80.29% in 2018 (from Wuhan Municipal Statistics Bureau). The discussion of the changes in UHI and its driving factors not only helps to mitigate UHI in Wuhan but also useful for other cities with severe thermal environments and rapid urbanization. In summary, there are two objectives in this study. The first objective is to investigate the spatiotemporal patterns of UHI in Wuhan during 2001~2018 and also the UHI intensity changes in 13 administrative regions, respectively. The second one is to compare the fitting effect of SEM and OLS models and to analyze the driving factors of UHI and their explanatory power changes in Wuhan during the 18 years.

Materials and methods

Study area

Wuhan is the central city of China, and the capital of Hubei Province, located between 113°41′~115°05′E and 29°58′ ~ 31°22′N, with an area of 8569.15 km2 and a permanent population of 11.081 million (2018). Wuhan is in the hot summer and cold winter zone, with a subtropical monsoon climate. Freshwater resources are abundant. Wetland resources rank top 3 among inland cities in China. The Yangtze River and Hanshui converge in the center of Wuhan with numerous lakes surround them. There are 13 administrative Districts, including 7 central urban areas (Jiang'an District, Jianghan District, Qiaokou District, Hanyang District, Qingshan District, Hongshan District, and Wuchang District) and 6 new urban areas (Huangpi District, Xinzhou District, Dongxihu District, Caidian District, Hannan District, and Jiangxia District), the geographical distribution is shown in **Fig. 1**.

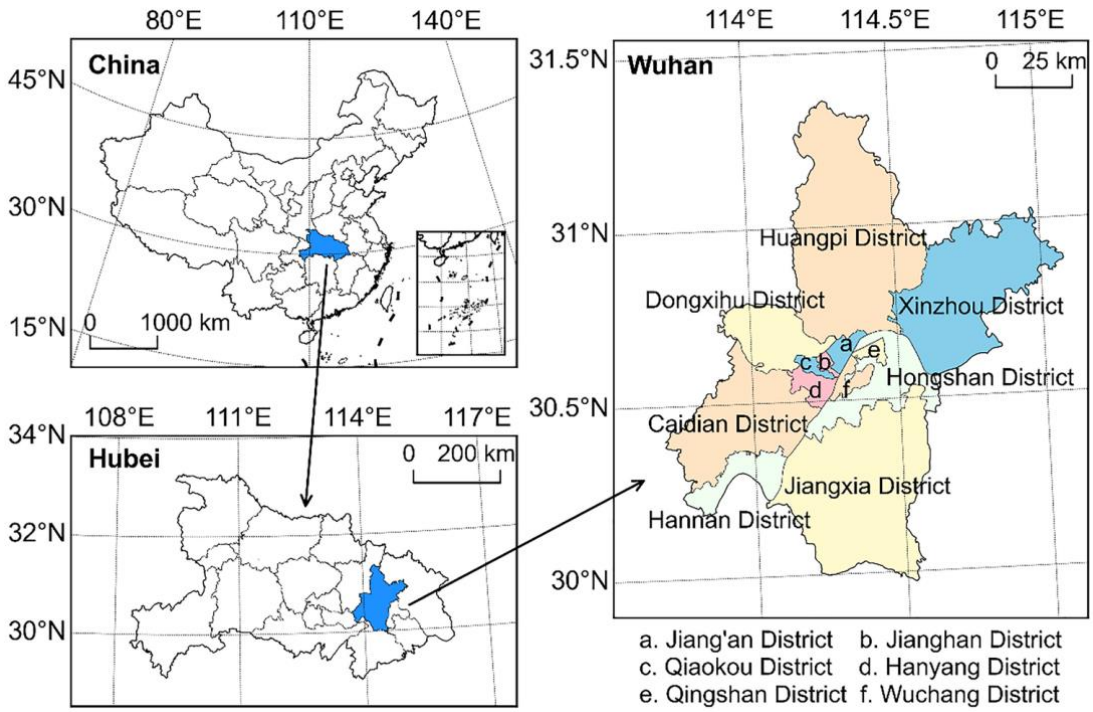

Fig.1. **The location and geographical divisions of Wuhan**

Data collection

Satellite data and other auxiliary data

MOD11A2 V6 product is used to obtain the daytime LST in Wuhan in summer (June, July, and August) during 2001~2018. MODIS (moderate resolution imaging spectroradiometer) is aboard the Terra satellite. MOD11A1 product uses the split window algorithm to obtain the daily LST under cloud-free conditions, which is in 10:30 and 22:30 local time. MOD11A2 V6 product calculates the average surface temperature in 8 days using MOD11A1 with a spatial resolution of 1 km. The accuracy of the LST is higher than 1°C in the range of − 10 ~ 50 °C (Wan 2008). MCD12Q1 V6 product is used to obtain the land cover data. It provides global land cover types at yearly intervals from 2001 to 2018, with a spatial resolution of 500 m. The IGBP (Annual International Geosphere-Biosphere Programme classification) classification scheme is used. Landsat is a joint project of the United States Geological Survey (USGS) and the National Aeronautics and Space Administration (NASA). The satellite acquires a complete world map every 16 days with a resolution of 30 m. Landsat5 is used to obtain NDVI, NDBI, and MNDWI from 2000 to 2011, and Landsat8 is used to obtain these indices from 2013 to 2018. The data in 2012 has not been applied in this study

because of the data quality. The Defense Meteorological Satellite Program Operational Line-Scan System (DMSP-OLS) provides stable nighttime light data from 1992 to 2013. The national polar-orbiting partnership-visible infrared imaging radiometer suite (NPP-VIIRS) provides nighttime light data from 2012 to the present. A fusion data proposed by Chen et al. (Chen et al. 2021) is used, which has a high accuracy and can monitor the state of economic activities over a long time series. Different types of population data can be obtained in WorldPop. The unconstrained individual countries 2000–2020 UN adjusted data is employed. This dataset uses a top–down method to predict population numbers by collecting census data and then adjust to match United Nations national population estimates. Elevation data is obtained from Advanced Spaceborne Thermal Emission and Refection Radiometer (ASTER) Global Digital Elevation Model Version 3 (GDEM 003) (NASA/METI/AIST/Japan Spacesystems and U.S./Japan ASTER Science Team 2019). It is used to avoid the effect of elevation on temperature in the UHI intensity calculations (Table 1).

Preprocessing

Google Earth Engine is a visual geographic analysis platform that stores a variety of satellite remote sensing data with long time series and provides algorithms to deal with the dataset. MOD11A2 product is obtained, and then, the mean daytime LST is calculated during June, July, and August through Google Earth Engine using **Eq. (1)**.

$$LST = 0.02DN - 273.15 \quad (1)$$

where DN is the pixel gray value.

Three indices are calculated in Google Earth Engine, and the mean value in summer is obtained as well. The influence of clouds is removed by the quality assessment band in Landsat product before the calculation of three indices. The formulas are shown in **Table 2**.

Table 1 Data sources and descriptions

Product	Period	Spatial resolution (m)	Data type	Source
MOD11A2	Summer of 2001~2018 (June, July, and August)	1000	LST (°C)	NASA(https://search.earthdata.nasa.gov/search)
MCD12Q1	2001~2018	500	Land cover	NASA(https://search.earthdata.nasa.gov/search)
Landsat5	Summer of 2001~2011 (June, July, and August)	30	NDVI, NDBI, MNDWI	USGS(https://earthexplorer.usgs.gov/)
Landsat8	Summer of 2013~2018 (June, July, and August)	30	NDVI, NDBI, MNDWI	USGS(https://earthexplorer.usgs.gov/)
DMSP-OLS, NPP-VIIRS	2001~2018	~500	Nighttime light (nW/(cm^2·sr)	https://doi.org/10.7910/DVN/YGIVCD
-	2001~2018	1000	Population (person)	https://www.worldpop.org
ASTER GDEM V003	-	~30	Elevation (m)	https://asterweb.jpl.nasa.gov/gdem.asp

Table 2 The formula of NDVI, MNDWI, and NDBI

Index	Formula	Landsat5	Landsat8
NDVI	$\frac{NIR-RED}{NIR+RED}$	$\frac{Band4-Band3}{Band4+Band3}$	$\frac{Band5-Band4}{Band5+Band4}$
MNDWI	$\frac{GREEN-SWIR}{GREEN+SWIR}$	$\frac{Band2-Band5}{Band2+Band5}$	$\frac{Band3-Band6}{Band3+Band6}$
NDBI	$\frac{SWIR-NIR}{SWIR+NIR}$	$\frac{Band5-Band4}{Band5+Band4}$	$\frac{Band6-Band5}{Band6+Band5}$

Note: *NIR*, near-infrared band; *RED*, red band; *GREEN*, green band; *SWIR*, shortwave infrared band

Methods

Mean standard deviation

The mean standard deviation method can reflect the spatial variation of LST (Liu et al. 2016). The method is therefore used to classify LST. And it is divided into 5 types, including low-temperature zone, sub-low-temperature zone, medium-temperature zone, sub-high-temperature zone, and high-temperature zone. The classification standards are shown in **Table 3**.

Calculation of UHI intensity

The UHI intensity is usually calculated by the temperature difference between urban and suburban areas. It is defined as follows:

$$\Delta T = T_i - T_0 \tag{2}$$

where Ti is the LST of each pixel, T0 is the average LST of the areas where the NDVI is greater than 0.6 or the NDWI is greater than 0.3 according to Lin et al. (Lin et al. 2018). Because the modified normalized difference water index (MNDWI) is more accurate than NDWI (Xu 2006), MMDWI is used instead of NDWI. In addition, to

reduce the effect of elevation on temperature, it is ensured that the difference in elevation between urban and suburban areas does not exceed 50 m.

Table 3 The classification standards of temperature zones

Standard	Temperature zones
$t \leq T$-std	Low-temperature zone
T-std $< t \leq T$-0.5std	Sub-low-temperature zone
T-0.5std $< t \leq T + 0.5$std	Medium-temperature zone
$T + 0.5$std $< t \leq T +$ std	Sub-high-temperature zone
$T +$ std $< t$	High-temperature zone

Note: t is the LST of each pixel, T is the average LST, and std is the standard deviation of LST

In order to have a better understanding of the urban thermal environment in Wuhan, only the human settlements are taken into consideration. The UHI intensity in built-up land is calculated.

Spatial autocorrelation

Moran's *I* is widely used to calculate spatial autocorrelation, including global Moran's *I* and Local Moran's *I*. The global Moran's *I* can be used to measure the spatial clustering or dispersion characteristics. The local Moran's *I* shows the contribution of each observation (Anselin 1995), which can be used to explore the spatial clustering or dispersion characteristics of a local region. The global Moran's I can be calculated by **Eq. (3).**

$$\text{Moran}'\text{s } I = \frac{n\sum_i\sum_j W_{ij}\left(x_i - \bar{x}\right)\left(x_j - \bar{x}\right)}{\sum_i\sum_j W_{ij}\sum_i\left(x_i - \bar{x}\right)^2} \tag{3}$$

Global Moran's *I* ranges from − 1 to 1. Values greater than 0 suggests spatial clustering; values less than 0 suggests spatial dispersion; values equal to 0 suggests no spatial autocorrelation.

The local Moran's *I* can be calculated by **Eq. (4).**

$$\text{Local Moran}'\text{s } I = \frac{n\left(x_i - \bar{x}\right)\sum_j W_{ij}\left(x_j - \bar{x}\right)}{\sum_i\left(x_i - \bar{x}\right)^2} \tag{4}$$

where n is the total number of spatial units, Wij is the spatial weight matrix, xi is the observed value of the unit at position i; xj is the observed value of the unit at position j; and x is the mean value of all spatial units. Given the spatial resolution of data and

related research (Peng et al. 2020; Wu et al. 2021), a 1 km × 1 km fish net is constructed by GIS, and the average UHI intensity in the grid is calculated. Through the establishment of a spatial weight matrix in the GeoDa software, which is the queen adjacency, the spatial correlation analysis of UHI intensity from 2001 to 2018 (excluding 2012) is carried out.

Spatial error model and ordinary least squares model

In order to analyze the driving factors of UHI intensity and their influence changes, SEMs and OLS models are established and their fitting effect are compared. The correlation of error terms is considered in SEM. It can eliminate the interference of spatial autocorrelation and get accurate estimation results and statistical theories (Wang et al. 2019). It is calculated with **Eq. (5).** The OLS can be used to quantitatively analyze the linear correlation between two or more independent variables and dependent variables. It is expressed by **Eq. (6)**.

$$y = x\beta + \gamma W_{\varepsilon} + \mu \quad (5)$$

$$y = x\beta + b \quad (6)$$

where y is the dependent variable, x is the independent variable, β is the regression coefficient, γ is the spatial autoregressive coefficient of the error term, Wε is the spatial weight matrix, μ is the random error term, and b is the intercept.

The objects of models are Jianghan, Qiaokou Districts, and Caidian District. To ensure sufficient data and obtain accurate results, Jianghan District and Qiaokou District, which are geographically connected and similar in UHI intensity, are integrated into one object. Jianghan and Qiaokou Districts represent central urban area, which development tends to be saturated; Caidian District represents new urban area, with sufficient development momentum. The mean value of five independent variables including NDVI, NDBI, MNDWI, population, and nighttime light are calculated with a fish net of 1 km × 1 km. At the same time, the collinearity diagnosis of 5 independent variables is carried out to avoid multicollinearity. MNDWI is eliminated to ensure VIF < 5. All data are normalized before performing the regression analysis. SEMs and OLS models are established using GeoDa. Log likelihood (LogL), Akaike info criterion (AIC), Schwarz criterion (SC), and determination coefficient (R2) can reflect the fitting effect of SEMs and OLS models (Guo et al. 2020a). The larger the LogL and R^2, the smaller the AIC and SC, the better the fitting effect.

Results

The spatiotemporal pattern of UHI

The average and standard deviation of LST in Wuhan over 18 years are shown in Table 4. The average LST for each year in summer of Wuhan is between 29 and 32 ℃ and reaches a maximum of 31.34 ℃ in 2013. During 2001 to 2018, the average LST in Wuhan increases slightly. The average LST in 2014~2018 has increased by about 0.3 ℃ compared with that in 2001~2005. The standard deviation of LST has also increased. The LST distribution is becoming more and more uneven, mainly manifested by the increase in the critical temperature of high-temperature zone and sub-high-temperature zone, which has risen by about 0.5 ℃ and 0.4 ℃, respectively. The critical temperature of sub-low temperature zone also increased slightly, which is about 0.1 ℃. But the critical temperature of low-temperature zone doesn't change much. Fig. 2 shows the spatiotemporal patterns of LST in Wuhan during 2001~2018. The high-temperature zones are first located at the central areas, like Jianghan District, Qiaokou District, Hanyang District, Jiang'an District, Wuchang District, and Qingshan District. The sub-high-temperature zones are scattered around the high-temperature zones and are located at some small urban areas. High-temperature zone expands to the surrounding areas year by year and connects with sub-high-temperature zones, which area increases by about 496.15 km^2. The northern Wuhan, where the land type is mainly savannas, croplands, and forests and the LST is lower than the central area, shifted from high- or sub-high-temperature zones to medium or low temperature zones during 2001-2018. High temperature zones in central area expand, and the average LST in Wuhan increases from 2001 to 2018, while the LST in northern area does not change much, resulting in the change from high-temperature zone to low-temperature zone in northern Wuhan. The distribution pattern of high-temperature zone has changed from scattered distribution to concentrated and contiguous distribution. The high-temperature zones are mainly transformed from sub-high-temperature zones. The proportion of medium-temperature zone, sub-low-temperature zone, and low-temperature zone do not change much. Low-temperature zones and sub-low-temperature zones are mainly distributed in the city fringe which are water bodies, croplands, and forests.

Table 4 The average and standard deviation of LST in Wuhan during 2001~2018

Year	T (°C)	std	T-std (°C)	T-0.5std (°C)	T + 0.5std (°C)	T + std (°C)
2001	30.73	1.75	28.98	29.85	31.61	32.48
2002	30.53	1.55	28.98	29.75	31.30	32.08
2003	30.83	1.75	29.08	29.96	31.70	32.58
2004	29.62	1.43	28.19	28.90	30.34	31.05
2005	30.09	1.63	28.47	29.28	30.91	31.72
2006	30.62	1.76	28.86	29.74	31.50	32.38
2007	29.71	1.50	28.21	28.96	30.46	31.21
2008	29.45	1.46	27.99	28.72	30.19	30.92
2009	30.81	1.83	28.99	29.90	31.73	32.64
2010	30.02	1.66	28.36	29.19	30.85	31.67
2011	29.73	1.73	28.01	28.87	30.60	31.46
2012	30.45	1.94	28.51	29.48	31.42	32.39
2013	31.34	1.91	29.43	30.39	32.29	33.25
2014	30.20	1.63	28.57	29.39	31.02	31.84
2015	30.39	1.90	28.49	29.44	31.35	32.30
2016	30.34	1.77	28.57	29.45	31.22	32.11
2017	30.75	2.11	28.65	29.70	31.81	32.86
2018	31.23	1.96	29.27	30.25	32.21	33.19

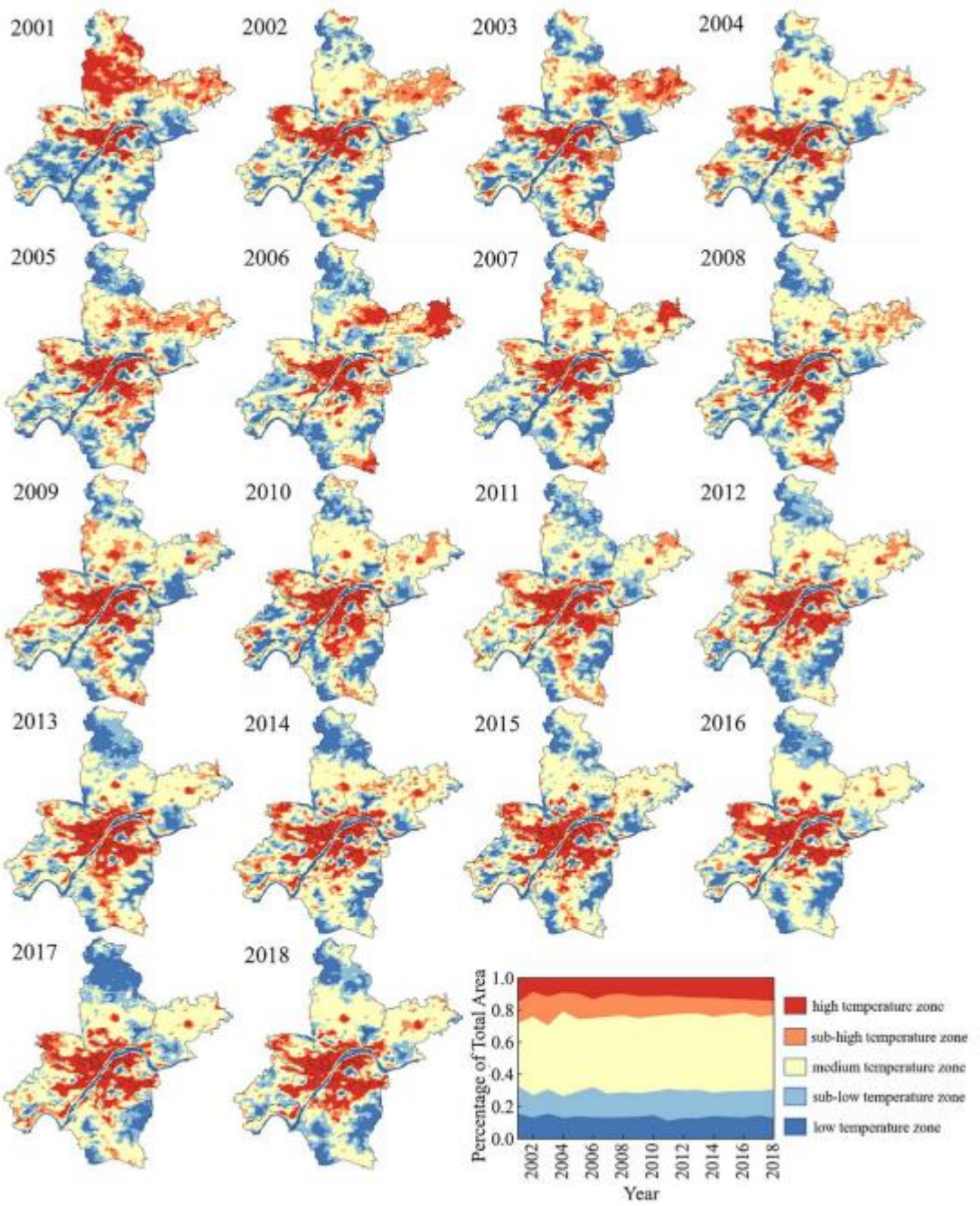

Fig. 2. The spatiotemporal patterns of LST in Wuhan during 2001~2018

The changes of UHI intensity

The UHI intensity changes of built-up land are determined, as shown in Fig. 3. The UHI intensity in 2012 is obtained by interpolation. The average LST for each year in Wuhan is around 32 ~ 35 °C. The average UHI intensity is around 3 ~ 4 °C and reaches the highest of 4.36 °C in 2011. Compared with UHI intensity in 2001~2005, the average value in 2014~2018 has increased by about 0.45 °C showing a slightly upward trend. The places with high UHI intensity in Wuhan are in the central urban areas. Jianghan District and Qiaokou District have the highest UHI intensity among all the central urban areas, which is 2 ~ 3 °C higher than the average level of Wuhan and 4 °C higher than

the areas with weak UHI intensity such as Huangpi District, Xinzhou District, and Hannan District. The UHI intensity in Jianghan District and Qiaokou District is about 6 ℃ and even reaches up to 7.57 ℃. However, the UHI intensity in Jianghan District has a decreasing trend after 2011. The UHI intensity is about 5.37 ℃ in recent years, which is 1 ℃ lower than that in 2001~2005. Changes in Wuchang District are similar to those in Jianghan District, and the UHI intensity begins to be lower than the average level of Wuhan. The UHI intensity changes of other central urban areas is similar to the average level in Wuhan. The UHI intensity in new urban areas is below the average value of Wuhan in general. But the intensity has increased over time and even shows a tendency to surpass that of the central urban areas. The UHI intensity in Dongxihu District and Caidian District has been higher than the average level of Wuhan in recent years. The UHI intensity of Caidian District has the most obvious change among all the new urban areas, with an increase of 1.70 ℃ in the last five years compared to 2001–2005. The highest intensity reaches up to 4.51 ℃. Xinzhou District has the smallest increase of about 0.63℃ among all the new urban areas, but it is still higher than the average level of Wuhan.

Spatial clusters of UHI intensity

Global Moran's I is calculated to investigate the spatial autocorrelation of UHI intensity. It is found that the global Moran's I is higher than 0.79 in all the 17 years (excluding 2012), the P value is less than 0.001, and the Z score is greater than 33, which means a strong spatial positive correlation. LISA (local indicators of spatial association) values can be used to get the local spatial correlation, as shown in **Fig. 4**. High–high clusters are mainly located at the central urban areas in 2001. During 18 years, high–high clusters gradually disperse and move to the city fringe. The UHI intensity of new urban areas such as Dongxihu District, Caidian District, and Jiangxia District has increased. It can be suggested that the UHI intensity in the central urban areas has weakened, and the UHI intensity in the new urban area has increased.

SEM results

The changes of four driving factors (NDVI, NDBI, population, and nighttime light) in Jianghan, Qiaokou, and Caidian Districts from 2001 to 2018 are first investigated, as shown in Fig. 5. The NDVI in Jianghan, Qiaokou Districts is lower than that of Caidian district, but the other three driving factors are higher, which means that Jianghan and Qiaokou Districts have less green space, more population, more human activities, and higher urbanization level. During 2001–2018, the population of Jianghan and Qiaokou Districts increased, the intensity of nighttime lights increased, and, in recent years, there is a trend toward more vegetation cover. For Caidian District, NDBI has increased and the intensity of nighttime lights has increased noticeably in recent years. But NDVI has a tendency to decrease. In general, the urbanization level of both is increasing, but the urbanization level of Jianghan and Qiaokou Districts is higher than that of Caidian

district. The change of NDVI shows that Jianghan and Qiaokou Districts are developing in a more sustainable way compared to Caidian district.

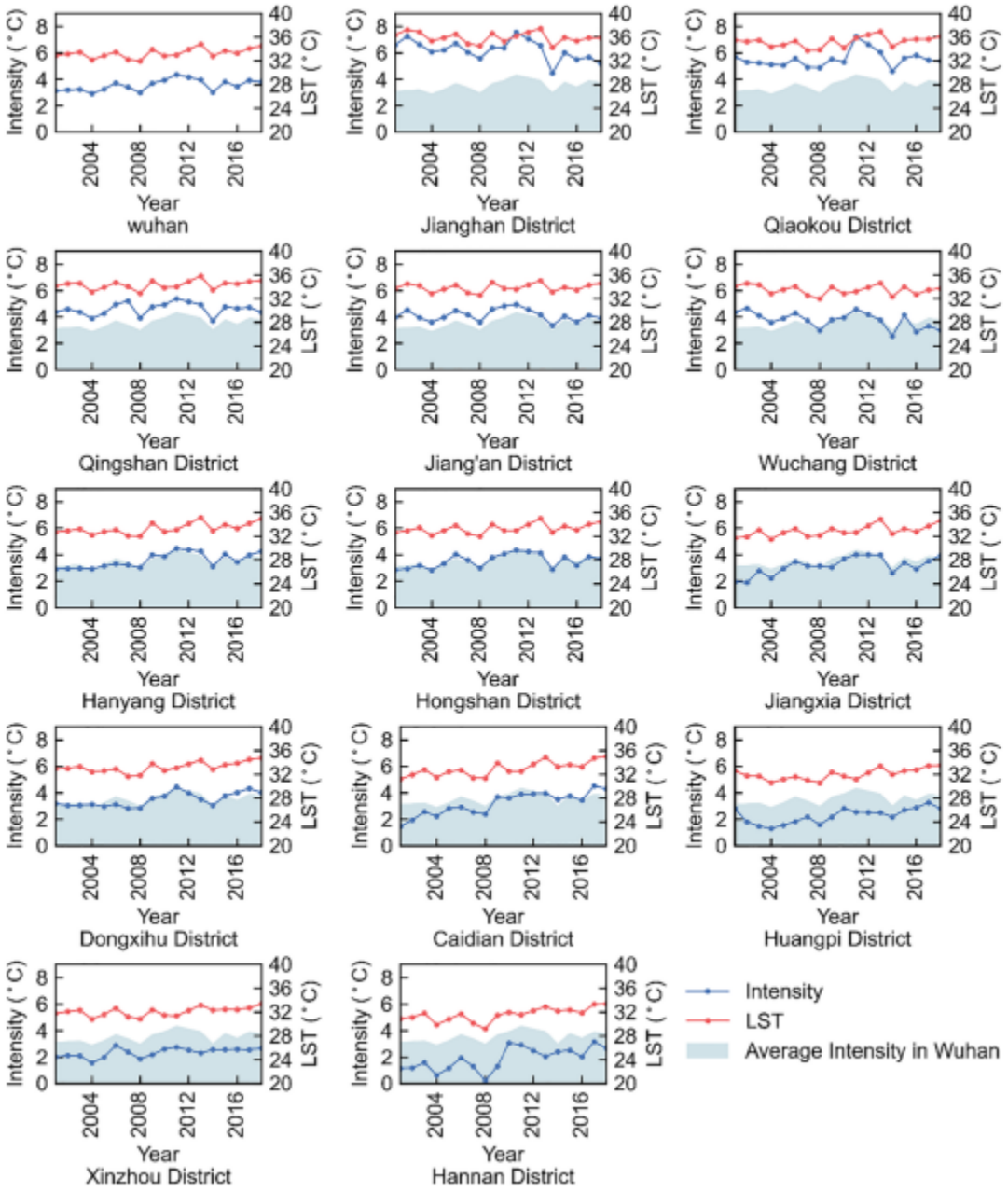

Fig. 3 The UHI intensity changes of Wuhan and its 13 administrative regions during 2001~2018

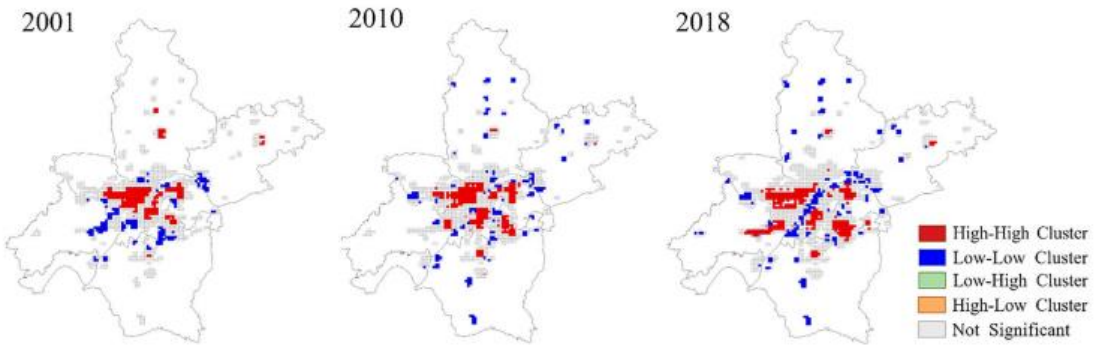

Fig. 4 The spatial clustering/dispersion characteristics of Wuhan in 2001, 2010, and 2018

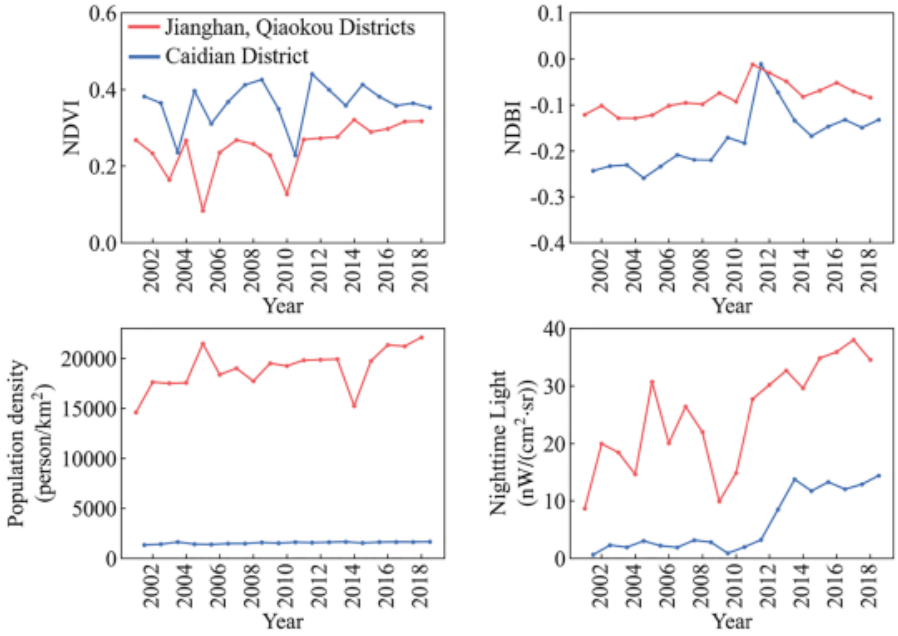

Fig. 5 Variations of NDVI, NDBI, population, and nighttime light from 2001 to 2018

From 2001 to 2018 (excluding 2012), 34 SEMs and 34 OLS models are established. Through the comparison of Log*L*, AIC, SC, and R^2 , the fitting effect of SEMs and OLS models can be analyzed. From Table 5 and 6, it is found that the Log*L* and R^2 in SEMs are larger than that in OLS models, and the AIC and SC in SEMs are smaller than those in OLS models. It means that the fitting effect of SEMs is better than OLS models for both Jianghan and Qiaokou Districts, and Caidian District for each year. Therefore, the results from SEMs are discussed. The coeffcient values of four driving factors (NDVI, NDBI, population, and nighttime light) in SEMs are shown in Fig. 6. For Jianghan and Qiaokou Districts, NDBI has the greatest impact on UHI intensity. For Caidian District, NDBI and nighttime light are the main factors driving the increase in surface temperature. It can be found that the relationship between NDVI and UHI intensity has

changed from a negative correlation to a positive correlation. And the positive correlation in Jianghan and Qiaokou Districts is more obvious than that in Caidian District. The influence of NDBI on UHI intensity has always been a significant positive influence, and the influence in Jianghan and Qiaokou Districts is greater than that in Caidian District. However, the influence of NDBI has begun to converge in recent years. The main manifestation is that the influence of NDBI on UHI intensity in Jianghan and Qiaokou Districts has become smaller. The influence of population and nighttime light on UHI intensity is quite different in Jianghan and Qiaokou Districts and Caidian District. For Caidian District, the greater the population, the denser the nighttime lights, the stronger the UHI intensity. There is a significant positive correlation between population and nighttime light and UHI intensity. For Jianghan and Qiaokou Districts, population and nighttime lights have little influence on UHI intensity. But in recent years, the nighttime light shows a significant positive correlation with UHI intensity.

Discussions

Driving factors of UHI intensity

Four driving factors (NDVI, NDBI, population, and night-time light) of UHI are considered by establishing SEMs. It is found that the relationship between NDVI and UHI intensity has changed from a negative correlation to a positive correlation. There may be three reasons through the analysis of original data. Firstly, when the NDVI is small, the land cover is mainly water body (Khamchiangta and Dhakal 2020), so the UHI intensity is low, which will lead to a positive correlation. Secondly, NDVI values are generally low. Mackey et al. found that NDVI showed a strong correlation with temperature only after a certain threshold was exceeded (Mackey et al. 2012); thus, the negative correlation trend has been weakened. Thirdly, the LST somewhere could be affected by the surrounding environment. The green land closed to construction land has high LST, which also contributes to a positive correlation. Keeratikasikorn et al. find that the mitigation effect of plants on LST is smaller in high-density building areas than in low-density building areas in Bangkok (Keeratikasikorn and Bonafoni 2018). This may be due to the increasing areal proportion of urban vegetation patches influenced by edge effect (Lin et al. 2018). Compared with Caidian District, Jianghan and Qiaokou Districts are more urbanized, and there is less vegetation and smaller NDVI (Fig. 5). Therefore, Jianghan and Qiaokou Districts show a higher positive relationship between NDVI and LST compared to Caidian District. As for NDBI, the influence of NDBI on UHI intensity is stable, which is significant for each year both in Jianghan, Qiaokou Districts and Caidian District. And the influence in Jianghan and Qiaokou Districts is greater than in Caidian District. It is also because of the high level of urbanization in Jianghan and Qiaokou Districts. In recent years, the impact of NDBI seems to have weakened in Jianghan and Qiaokou Districts, probably due to the decrease of NDBI and the increase of NDVI (Fig. 5), which will reduce LST and help

alleviate UHI intensity. Additionally, urban canyon can have an impact on UHI intensity and will behave differently in the central and new urban areas, due to the fact that the central city is more densely built and has more tall buildings. Sky view factor plays an important role in describing urban form, reflecting street geometry and building density. The larger the sky view factor, the more open the terrain is (Dirksen et al. 2019). Huang and Wang found that LST is positively correlated with sky view factor in areas with high-density and high-rise buildings, while in areas with low building density, SVF has little effect (Huang and Wang 2019). Tall buildings can form shadows to lower LST (Yu et al. 2021). Central urban area has taller and denser buildings, a smaller sky view factor, and more shadows formed by buildings, which can reduce the surface temperature to some extent. This may be another reason why the impact of NDBI on UHI weakens in central urban area. The relationship between social–economic factors and UHI intensity in central urban area and new urban area is quite different. Research shows that there is a logarithmic relationship between economic levels and UHI intensity (Cui et al. 2016). In the early stage of urbanization, there is a close relationship between population, nighttime lights and UHI intensity. However, the spatial heterogeneity of population and nighttime light decreases as urban development tends to be saturated; hence, the correlation between population, nighttime light, and UHI intensity in central urban area is smaller than in new urban area. In recent years, the impact of nighttime light on UHI intensity in central urban area becomes significant. The first areas with strong nighttime light are mainly along the river, which have a lower UHI intensity. In recent years, the nighttime lights have increased in areas far from the riverside, while the UHI intensity in these areas is high, so a positive correlation between nighttime lights and UHI intensity is shown in recent years.

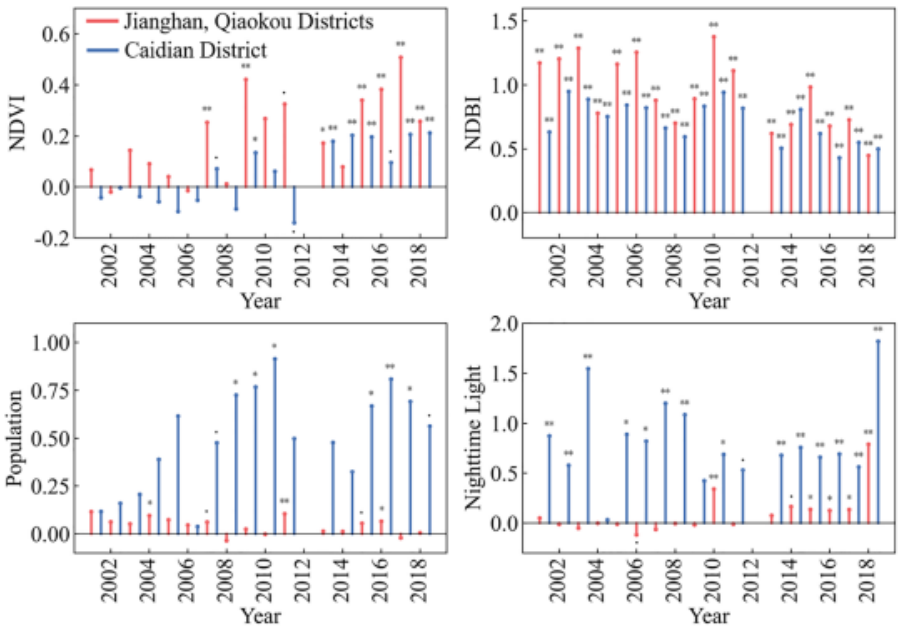

Fig. 6 Regression coefcient in SEM of NDVI, NDBI, population, and nighttime

light (P < 0.01, * P < 0.05, and·P < 0.1)**

Table 5 The fitting effect comparison of OLS models and SEMs in Jianghan and Qiaokou Districts during 2001~2018

	2001		2002		2003		2004	
	OLS	SEM	OLS	SEM	OLS	SEM	OLS	SEM
Log*L*	98.56	128.90	74.69	103.98	121.53	150.48	132.41	159.73
AIC	− 187.12	− 247.81	− 139.39	− 197.96	− 233.07	− 290.97	− 254.81	− 309.46
SC	− 175.40	− 236.09	− 128.44	− 187.02	− 220.68	− 278.58	− 242.54	− 297.19
R^2	0.67	0.89	0.72	0.93	0.72	0.89	0.74	0.90
	2005		2006		2007		2008	
	OLS	SEM	OLS	SEM	OLS	SEM	OLS	SEM
Log*L*	47.01	51.35	119.04	156.26	134.36	175.75	105.11	139.23
AIC	− 84.02	− 92.69	− 228.07	− 302.53	− 258.72	− 341.49	− 200.22	− 268.47
SC	− 76.69	− 85.36	− 215.63	− 290.09	− 246.34	− 329.10	− 188.50	− 256.75
R^2	0.32	0.64	0.71	0.91	0.69	0.91	0.46	0.84
	2009		2010		2011		2013	
	OLS	SEM	OLS	SEM	OLS	SEM	OLS	SEM
Log*L*	124.77	153.99	103.66	109.43	123.77	158.35	126.66	171.93
AIC	− 239.53	− 297.97	− 197.31	− 208.87	− 237.53	− 306.70	− 243.32	− 333.86
SC	− 227.50	− 285.94	− 186.52	− 198.08	− 225.14	− 294.32	− 230.88	− 321.42
R^2	0.66	0.88	0.64	0.75	0.51	0.84	0.59	0.89
	2014		2015		2016		2017	
	OLS	SEM	OLS	SEM	OLS	SEM	OLS	SEM
Log*L*	102.87	122.59	149.65	165.83	123.43	155.30	147.86	171.62
AIC	− 195.74	− 235.18	− 289.30	− 321.65	− 236.86	− 300.61	− 285.72	− 333.24
SC	− 185.02	− 224.47	− 277.14	− 309.50	− 225.08	− 288.82	− 273.45	− 320.97
R^2	0.43	0.78	0.72	0.85	0.38	0.80	0.50	0.78
	2018							
	OLS	SEM						
Log*L*	138.75	165.13						
AIC	− 267.51	− 320.27						
SC	− 255.41	− 308.17						
R^2	0.57	0.83						

Urban thermal environment in Wuhan during 2001~2018

The long-term spatiotemporal patterns of UHI in Wuhan during 2001~2018 are investigated. It can be found that the urban thermal environment in Wuhan is getting worse and the affected scope of UHI is getting larger. And the UHI intensity in the central urban areas has weakened while the UHI intensity in the new urban area has increased. Shen et al. (Shen et al. 2016) found that the high-temperature area within the old city zones showed a decreasing tendency during 1988–2013 in Wuhan. Gui et al. (Gui et al. 2019) find that the LST between urban and rural areas in Wuhan from 2001 to 2017 has increased, and the daytime ΔLST in summer is 0.106 °C/a in old urban area and 0.207 °C/a in urbanized area. The increasing rate of LST in old urban area is slower than that in urbanized area, which is consistent with our results. According to the driving factors of UHI intensity, the NDVI has increased and tall buildings have been constructed in Jianghan and Qiaokou Districts, which may explain the reason why there is a slow or even a negative UHI intensity change in central urban areas. In new urban area, it is still developing. More and more natural land has been converted into

impervious land, causing LST rise. However, although the UHI intensity in central urban area has declined, most of UHI intensity is still above 4 °C. The UHI intensity in new urban areas is relatively low, but the growth rate is fast. Regional heat island can be defined when the UHI intensity is higher than 2 °C (Qiu et al. 2017; Yu et al. 2019). It is found that the area of regional heat island in Wuhan increases from 63.4% in 2001 to 71.4% in 2018, which indicates that most of the living space has suffered from UHI. Hot environment will threaten the health and lives of residents. In a case study of Jiang'an District from 2003 to 2010, 1 °C increase in mean temperature above the hot thresholds will cause a 25.18% increase in non-accidental mortality (Zhang et al. 2016). The severe urban thermal environment in Wuhan will undoubtedly cause a large number of deaths. Moreover, the impact of high temperature on the elderly is more significant (Taylor et al. 2015; Zhang et al. 2017). China's aging population is deepening according to the results of the seventh national census. The ageing population (age ≥ 65) is 8.4261 million in Wuhan, and it is 2.5 million more than seven years ago, which will further amplify the adverse impact of hot environment. Therefore, it is urgent to implement corresponding mitigation strategies to improve the urban thermal environment. And it is also necessary to strengthen residents' awareness of environmental changes which will promote the implementation of relevant policies.

Table 6 The fitting effect comparison of OLS models and SEMs in Caidian District during 2001~2018

	2001		2002		2003		2004	
	OLS	SEM	OLS	SEM	OLS	SEM	OLS	SEM
Log*L*	202.21	279.55	231.42	279.29	208.70	248.03	219.92	270.75
AIC	− 394.41	− 549.09	− 452.83	− 548.58	− 407.41	− 486.07	− 429.85	− 531.51
SC	− 379.13	− 533.81	− 437.30	− 533.05	− 392.52	− 471.19	− 414.26	− 515.92
R^2	0.54	0.88	0.56	0.80	0.69	0.86	0.58	0.84
	2005		2006		2007		2008	
	OLS	SEM	OLS	SEM	OLS	SEM	OLS	SEM
Log*L*	166.63	201.78	224.57	260.28	271.28	295.43	197.20	228.41
AIC	− 323.25	− 393.57	− 439.14	− 510.55	− 532.55	− 580.86	− 384.40	− 446.82
SC	− 309.15	− 379.46	− 423.43	− 494.84	− 516.93	− 565.24	− 369.45	− 431.86
R^2	0.64	0.84	0.66	0.83	0.76	0.85	0.65	0.82
	2009		2010		2011		2013	
	OLS	SEM	OLS	SEM	OLS	SEM	OLS	SEM
Log*L*	230.60	260.56	180.06	237.70	200.31	241.33	234.05	284.82
AIC	− 451.19	− 511.12	− 350.12	− 465.40	− 390.62	− 472.66	− 458.10	− 559.63
SC	− − 435.79	− 495.71	− 334.72	− 449.99	− 375.28	− 457.31	− 442.30	− 543.84
R^2	0.69	0.83	0.55	0.84	0.61	0.82	0.73	0.88
	2014		2015		2016		2017	
	OLS	SEM	OLS	SEM	OLS	SEM	OLS	SEM
Log*L*	158.24	175.71	239.64	280.51	242.31	286.75	245.02	297.68
AIC	− 306.49	− 341.43	− 469.27	− 551.03	− 474.63	− 563.51	− 480.05	− 585.35
SC	− 292.81	− 327.75	− 453.45	− 535.20	− 458.89	− 547.77	− 463.79	− 569.09
R^2	0.67	0.80	0.71	0.85	0.68	0.85	0.68	0.86
	2018							
	OLS	SEM						
Log*L*	224.46	292.07						
AIC	− 438.92	− 574.14						
SC	− 422.84	− 558.06						
R^2	0.71	0.90						

UHI mitigation strategy

SEMs have been established to study the driving factors of UHI intensity. It is found that there is a positive correlation between NDVI and UHI intensity. Although there is the influence of water bodies, the reduction of NDVI range cannot be ignored, which indicates that more vegetation is needed. Additionally, the mitigation effect of plants on LST is relatively small in high-density building areas (Keeratikasikorn and Bonafoni 2018), meaning that the cooling effect of vegetation will be affected by adjacent areas. To decrease the effect of UHI, higher vegetation coverage is required to enhance the cooling effect. Broken green patches will limit its cooling effect (Li et al. 2013b). Continuous and complete green patches is needed. However, the area for greening in central urban areas is limited; hence, the alternatives of roof greening and vertical greening can be conducted. NDBI has the strongest influence on UHI intensity. In addition to using the transpiration of vegetation to remove heat, impervious pavement can be replaced with permeable pavements to reduce LST by evaporation of water (Li et al. 2013a). Promoting the construction of 'sponge city' will also play an important role in improving the urban thermal environment. Social-economic factors have different effects on Jianghan and Qiaokou Districts and Caidian District, which requires different mitigation strategies for central urban area and new urban area. It is found that

there is a more significant correlation between social–economic factors and UHI intensity in new urban area than in central urban area. To reduce population density and the brightness of nighttime lights, satellite cities can be established to share part of the population and urban functions, which can help to alleviate UHI. The development of central urban area has become saturated. Although high-rise buildings may not lead to a significant increase in UHI, the substantial reduction in wind speed is not conducive to UHI mitigation (Zhou and Chen 2018). The design of urban ventilation corridors can better the air circulation and is conducive to create a better living environment (Morris and Simmonds 2001).

Conclusions and outlook

Urban thermal environment has been changing along with urbanization. In this study, the dynamic change of LST in Wuhan during summer of 2001~2018 was uncovered. Then, the UHI intensity changes of built-up land in 13 administrative regions were determined respectively. Finally, the driving factors of UHI intensity and their explanatory power changes during 2001~2018 in central urban area and new urban area were investigated by SEMs. The following main conclusions can be drawn:

1. The LST of Wuhan is becoming more uneven, which is mainly manifested in the increase of the critical temperature of high-temperature zone (rises by about 0.5 ℃) and sub-high-temperature zone (rises by about 0.4 ℃). The distribution pattern of high-temperature zone has changed from scattered distribution to concentrated and contiguous distribution. The critical temperature of low-temperature zone does not change much.

2. The average UHI intensity in 2014~2018 has increased by about 0.45 ℃ compared to that in 2001~2005, showing a slightly upward trend. The central urban area shows the strongest UHI intensity which can reach up to 7.57 ℃. But in recent years, the ecological environment of some central urban areas such as Jianghan and Wuchang District have been improved while UHI intensity of new urban areas have been getting higher with a tendency to surpass that of the central area.

3. The fitting effect of SEMs is better than that of OLS models. The effects of driving factors vary between central urban area and new urban area. For Jianghan and Qiaokou Districts, NDBI has the greatest impact on UHI intensity. For Caidian District, NDBI and nighttime light are the main factors driving the increase in surface temperature. Social–economic factors (population and nighttime light) have a greater impact on new urban area than on central urban area. Moreover, the explanatory power has changed during 18 years. The influence of NDVI changes from negative to positive and the impact of NDBI in central urban area is weakened during 2001–2018.

During the urbanization process, the strategy for mitigating UHI should be different. Establishing satellite cities is an optimal solution for new urban area considering the great impact of social–economic factors. For central urban area, promoting the

construction of ‘sponge city’ and increasing green roofs and vertical greening as well as ventilation corridors are suitable. This study can offer insights into the formation and development of UHI which can better guide urban planning and management in Wuhan in the near future. In this study, the changes in explanatory power of the driving factors are analyzed using SEMs. Other driving factors, such as the urban landscape pattern, the three-dimensional indicators (building height and sky view factor), the meteorological factors and traffic levels will be investigated in the future work.

Author contribution

All authors contributed to the study conception and design. Material preparation, data collection, and analysis were performed by Xie Chen, Shicong Zhang, Zhiyong Tian, Yongqiang Luo, Jie Deng, and Jianhua Fan. The first draft of the manuscript was written by Xie Chen, and all authors commented on previous versions of the manuscript. All authors read and approved the final manuscript.

Funding

All the authors thank the financial support from the National Natural Science Foundation of China (No. 52208110), National Key R&D Program of China (no. 2021YFE0113500), Key R&D Program of Hubei Province (2022BAA028), the Fundamental Research Funds for the Central Universities, China (grant number: 2020kfyXJJS097), and Research Project of the Ministry of Housing and Urban-Rural Development of China “Research and Demonstration of Optimal Configuration of Energy Storage System in Nearly Zero Energy Communities”(K20210466), Research of Low carbon and zero carbon building design methodology and key technology of CABR (No. 20220109330730005).

Data availability

The data and materials that support the findings of this study are available from the corresponding author upon reasonable request.

Declarations of competing interests

The authors declare no competing interest.

References

Anselin L (1995) Local indicators of spatial association—LISA. Geogr Anal 27:93–115. https://doi.org/10.1111/j.1538-4632.1995.tb00338.x

Boegh E, Soegaard H, Hanan N et al (1999) A remote sensing study of the NDVI-T(s) relationship and the transpiration from sparse vegetation in the sahel based on high-resolution satellite data. Remote Sens Environ 69:224–240. https://doi.org/10.1016/S0034-4257(99)00025-5

Bottyán Z, Unger J (2003) A multiple linear statistical model for estimating the mean maximum urban heat island. Theor Appl Climatol 75:233–243. https://doi.org/10.1007/s00704-003-0735-

7

Carlson TN, Gillies RR, Perry EM (1994) A method to make use of thermal infrared temperature and NDVI measurements to infer surface soil water content and fractional vegetation cover. Remote Sens Rev 9:161–173. https://doi.org/10.1080/02757259409532220

Chen Z, Yu B, Yang C et al (2021) An extended time series (2000-2018) of global NPP-VIIRS-like nighttime light data from a cross-sensor calibration. Earth Syst Sci Data 13:889–906. https://doi.org/10.5194/essd-13-889-2021

Cui Y, Xu X, Dong J, Qin Y (2016) Influence of urbanization factors on surface urban heat island intensity: a comparison of countries at different developmental phases. Sustainability 8:706. https://doi.org/10.3390/su8080706

Dirksen M, Ronda RJ, Theeuwes NE, Pagani GA (2019) Sky view factor calculations and its application in urban heat island studies. Urban Clim 30:100498. https://doi.org/10.1016/j.uclim.2019.100498

Feng Y, Gao C, Tong X et al (2019) Spatial patterns of land surface temperature and their influencing factors: a case study in Suzhou. China. Remote Sens 11:182. https://doi.org/10.3390/rs11020182

Goward SN, Xue Y, Czajkowski KP (2002) Evaluating land surface moisture conditions from the remotely sensed temperature/vegetation index measurements: an exploration with the simplified simple biosphere model. Remote Sens Environ 79:225–242. https://doi.org/10.1016/S0034-4257(01)00275-9

Grigoraș G, Urițescu B (2019) Land use/land cover changes dynamics and their effects on surface urban heat island in Bucharest, Romania. Int J Appl Earth Obs Geoinf 80:115–126. https://doi.org/10.1016/j.jag.2019.03.009

Guha S, Govil H, Diwan P (2019) Analytical study of seasonal variability in land surface temperature with normalized difference vegetation index, normalized difference water index, normalized difference built-up index, and normalized multiband drought index. J Appl Remote Sens 13:1. https://doi.org/10.1117/1.jrs.13.024518

Gui X, Wang L, Yao R et al (2019) Investigating the urbanization process and its impact on vegetation change and urban heat island in Wuhan, China. Environ Sci Pollut Res 26:30808–30825. https://doi.org/10.1007/s11356-019-06273-w

Guo A, Yang J, Xiao X et al (2020a) Influences of urban spatial form on urban heat island effects at the community level in China. Sustain Cities Soc 53:101972. https://doi.org/10.1016/j.scs.2019.101972

Guo J, Han G, Xie Y et al (2020b) Exploring the relationships between urban spatial form factors and land surface temperature in mountainous area: a case study in Chongqing city. China. Sustain Cities Soc 61:102286. https://doi.org/10.1016/j.scs.2020.102286

Haase D, Nuissl H (2007) Does urban sprawl drive changes in the water balance and policy?. The case of Leipzig (Germany) 1870-2003. Landsc Urban Plan 80:1–13. https://doi.org/10.1016/j.landurbplan.2006.03.011

Hao Y, Zheng S, Zhao M et al (2020) Reexamining the relationships among urbanization, industrial structure, and environmental pollution in China—new evidence using the dynamic threshold panel model. Energy Reports 6:28–39. https://doi.org/10.1016/j.egyr.2019.11.029

Hu Y, Hou M, Jia G et al (2019) Comparison of surface and canopy urban heat islands within megacities of eastern China. ISPRS J Photogramm Remote Sens 156:160–168. https://doi.org/10.1016/J.ISPRSJPRS.2019.08.012

Huang X, Wang Y (2019) Investigating the effects of 3D urban morphology on the surface urban heat island effect in urban functional zones by using high-resolution remote sensing data: a case study of Wuhan, Central China. ISPRS J Photogramm Remote Sens 152:119–131. https://doi.org/10.1016/j.isprsjprs.2019.04.010

Hughes AC (2017) Understanding the drivers of Southeast Asian biodiversity loss. Ecosphere 8:e01624. https://doi.org/10.1002/ecs2.1624

Jiang L, Young MH, Hardee K (2008) Population,urbanization and the environment. World Watch, pp 34–39

Karakuş CB (2019) The impact of land use/land cover (LULC) changes on land surface temperature in Sivas city center and its surroundings and assessment of urban heat island. Asia-Pacific J Atmos Sci 55:669–684. https://doi.org/10.1007/s13143-019-00109-w

Keeratikasikorn C, Bonafoni S (2018) Urban heat island analysis over the land use zoning plan of Bangkok by means of Landsat 8 imagery. Remote Sens 10:440. https://doi.org/10.3390/rs10030440

Khamchiangta D, Dhakal S (2020) Time series analysis of land use and land cover changes related to urban heat island intensity: case of Bangkok Metropolitan Area in Thailand. J Urban Manag 9:383–395. https://doi.org/10.1016/j.jum.2020.09.001

Kim JH, Gu D, Sohn W et al (2016) Neighborhood landscape spatial patterns and land surface temperature: an empirical study on single-family residential areas in Austin, Texas. Int J Environ Res Public Health 13:880. https://doi.org/10.3390/ijerph13090880

Li H, Harvey JT, Holland TJ, Kayhanian M (2013a) The use of reflective and permeable pavements as a potential practice for heat island mitigation and stormwater management. Environ Res Lett 8:015023. https://doi.org/10.1088/1748-9326/8/1/015023

Li X, Zhou W, Ouyang Z (2013b) Relationship between land surface temperature and spatial pattern of greenspace: what are the effects of spatial resolution? Landsc Urban Plan 114:1–8. https://doi.org/10.1016/j.landurbplan.2013.02.005

Li Y, Sun Y, Li J, Gao C (2020) Socioeconomic drivers of urban heat island effect: empirical evidence from major Chinese cities. Sustain Cities Soc 63:102425. https://doi.org/10.1016/j.scs.2020.102425

Li YY, Zhang H, Kainz W (2012) Monitoring patterns of urban heat islands of the fast-growing Shanghai metropolis, China: using time-series of Landsat TM/ETM+ data. Int J Appl Earth Obs Geoinf 19:127–138. https://doi.org/10.1016/j.jag.2012.05.001

Lin Y, Jim CY, Deng J, Wang Z (2018) Urbanization effect on spatiotemporal thermal patterns and changes in Hangzhou (China). Build Environ 145:166–176. https://doi.org/10.1016/j.buildenv.2018.09.020

Liu G, Zhang Q, Li G, Doronzo DM (2016) Response of land cover types to land surface temperature derived from Landsat-5 TM in Nanjing Metropolitan Region, China. Environ Earth Sci 75:1–12. https://doi.org/10.1007/s12665-016-6202-4

Liu H, He X, Bai Y et al (2021a) Nightlight as a proxy of economic indicators: fine-grained GDP

inference around mainland China via attention-augmented CNN from daytime satellite imagery. Remote Sens 13:2067. https://doi.org/10.3390/rs13112067

Liu H, Huang B, Zhan Q et al (2021b) The influence of urban form on surface urban heat island and its planning implications: evidence from 1288 urban clusters in China. Sustain Cities Soc 71:102987. https://doi.org/10.1016/j.scs.2021.102987

Lu Y, Yue W, Huang Y (2021a) Effects of land use on land surface temperature: a case study of Wuhan, China. Int J Environ Res Public Health 18. https://doi.org/10.3390/ijerph18199987

Lu Y, Yue W, Liu Y, Huang Y (2021b) Investigating the spatiotemporal non-stationary relationships between urban spatial form and land surface temperature: a case study of Wuhan. China. Sustain Cities Soc 72:103070. https://doi.org/10.1016/j.scs.2021.103070

Ma T, Zhou C, Pei T et al (2012) Quantitative estimation of urbanization dynamics using time series of DMSP/OLS nighttime light data: a comparative case study from China's cities. Remote Sens Environ 124:99–107. https://doi.org/10.1016/j.rse.2012.04.018

Macintyre HL, Heaviside C (2019) Potential benefits of cool roofs in reducing heat-related mortality during heatwaves in a European city. Environ Int 127:430–441. https://doi.org/10.1016/j.envint.2019.02.065

Mackey CW, Lee X, Smith RB (2012) Remotely sensing the cooling effects of city scale efforts to reduce urban heat island. Build Environ 49:348–358. https://doi.org/10.1016/j.buildenv.2011.08.004

Monteiro FF, Gonçalves WA, de MB AL et al (2021) Assessment of urban heat islands in Brazil based on MODIS remote sensing data. Urban Clim 35:100726. https://doi.org/10.1016/j.uclim.2020.100726

Morabito M, Crisci A, Messeri A et al (2016) The impact of built-up surfaces on land surface temperatures in Italian urban areas. Sci Total Environ 551–552:317–326. https://doi.org/10.1016/j.scitotenv.2016.02.029

Morris CJG, Simmonds I (2001) Quantification of the influence of wind and cloud on the nocturnal urban heat island of a large city. J Appl Meteorol 40:169–182

NASA/METI/AIST/Japan Spacesystems and U.S./Japan ASTER Science Team (2019) ASTER global digital elevation model V003 [data set]. NASA EOSDIS Land Processes DAAC. https://doi.org/10.5067/ASTER/ASTGTM.003

Pathak C, Chandra S, Maurya G et al (2021) The effects of land indices on thermal state in surface urban heat island formation: a case study on Agra City in India using remote sensing data (1992–2019). Earth Syst Environ 5:135–154. https://doi.org/10.1007/s41748-020-00172-8

Peng J, Qiao R, Liu Y et al (2020) A wavelet coherence approach to prioritizing influencing factors of land surface temperature and associated research scales. Remote Sens Environ 246:111866. https://doi.org/10.1016/j.rse.2020.111866

Pichierri M, Bonafoni S, Biondi R (2012) Satellite air temperature estimation for monitoring the canopy layer heat island of Milan. Remote Sens Environ 127:130–138. https://doi.org/10.1016/J.RSE.2012.08.025

Qiu GY, Zou Z, Li X et al (2017) Experimental studies on the effects of green space and evapotranspiration on urban heat island in a subtropical megacity in China. Habitat Int 68:30–42. https://doi.org/10.1016/j.habitatint.2017.07.009

Shen H, Huang L, Zhang L et al (2016) Long-term and fine-scale satellite monitoring of the urban heat island effect by the fusion of multi-temporal and multi-sensor remote sensed data: a 26-year case study of the city of Wuhan in China. Remote Sens Environ 172:109–125. https://doi.org/10.1016/j.rse.2015.11.005

Shi W, Hou J, Shen X, Xiang R (2022) Exploring the spatio-temporal characteristics of urban thermal environment during hot summer days: a case study of Wuhan. China. Remote Sens 14. https://doi.org/10.3390/rs14236084

Sun Y, Wang S, Wang Y (2020) Estimating local-scale urban heat island intensity using nighttime light satellite imageries. Sustain Cities Soc 57:102125. https://doi.org/10.1016/j.scs.2020.102125

Taylor J, Wilkinson P, Davies M et al (2015) Mapping the effects of urban heat island, housing, and age on excess heat-related mortality in London. Urban Clim 14:517–528. https://doi.org/10.1016/j.uclim.2015.08.001

Taylor JR (2015) The China dream is an urban dream: assessing the CPC's national new-type urbanization plan. J Chinese Polit Sci 20:107–120. https://doi.org/10.1007/s11366-015-9341-7

Tobler WR (1970) A computer movie simulating urban growth in the Detroit region. Econ Geogr 46:234. https://doi.org/10.2307/143141

van Heerwaarden CC, de Arellano JVG (2008) Relative humidity as an indicator for cloud formation over heterogeneous land surfaces. J Atmos Sci 65:3263–3277. https://doi.org/10.1175/2008JAS2591.1

Wan Z (2008) New refinements and validation of the MODIS land-surface temperature/emissivity products. Remote Sens Environ 112:59–74. https://doi.org/10.1016/j.rse.2006.06.026

Wang L, Hou H, Weng J (2020) Ordinary least squares modelling of urban heat island intensity based on landscape composition and configuration: a comparative study among three megacities along the Yangtze River. Sustain Cities Soc 62:102381. https://doi.org/10.1016/j.scs.2020.102381

Wang WC, Chang YJ, Wang HC (2019) An application of the spatial autocorrelation method on the change of real estate prices in Taitung city. ISPRS Int J Geo-Information 8:249. https://doi.org/10.3390/ijgi8060249

Wu W, Li L, Li C (2021) Seasonal variation in the effects of urban environmental factors on land surface temperature in a winter city. J Clean Prod 299:126897. https://doi.org/10.1016/j.jclepro.2021.126897

Xu H (2006) Modification of normalised difference water index (NDWI) to enhance open water features in remotely sensed imagery. Int J Remote Sens 27:3025–3033. https://doi.org/10.1080/01431160600589179

Yang Q, Huang X, Tang Q (2019) The footprint of urban heat island effect in 302 Chinese cities: temporal trends and associated factors. Sci Total Environ 655:652–662. https://doi.org/10.1016/j.scitotenv.2018.11.171

Yang X, Peng LLH, Jiang Z et al (2020) Impact of urban heat island on energy demand in buildings: local climate zones in Nanjing. Appl Energy 260:114279. https://doi.org/10.1016/j.apenergy.2019.114279

Yi K, Tani H, Li Q et al (2014) Mapping and evaluating the urbanization process in Northeast China

using DMSP/OLS nighttime light data. Sensors 14:3207–3226. https://doi.org/10.3390/s140203207

Yin C, Yuan M, Lu Y et al (2018) Effects of urban form on the urban heat island effect based on spatial regression model. Sci Total Environ 634:696–704. https://doi.org/10.1016/j.scitotenv.2018.03.350

Yu X, Liu Y, Zhang Z, Xiao R (2021) Influences of buildings on urban heat island based on 3D landscape metrics: an investigation of China's 30 megacities at micro grid-cell scale and macro city scale. Landsc Ecol 1–20. https://doi.org/10.1007/s10980-021-01275-x

Yu Z, Yao Y, Yang G et al (2019) Spatiotemporal patterns and characteristics of remotely sensed region heat islands during the rapid urbanization (1995–2015) of Southern China. Sci Total Environ 674:242–254. https://doi.org/10.1016/j.scitotenv.2019.04.088

Yue W, Liu X, Zhou Y, Liu Y (2019) Impacts of urban configuration on urban heat island: an empirical study in China mega-cities. Sci Total Environ 671:1036–1046. https://doi.org/10.1016/j.scitotenv.2019.03.421

Zhang L (2008) Conceptualizing China's urbanization under reforms. Habitat Int 32:452–470. https://doi.org/10.1016/j.habitatint.2008.01.001

Zhang Y, Feng R, Wu R et al (2017) Global climate change: impact of heat waves under different definitions on daily mortality in Wuhan. China. Glob Heal Res Policy 2:10. https://doi.org/10.1186/s41256-017-0030-2

Zhang Y, Li C, Feng R et al (2016) The short-term effect of ambient temperature on mortality in Wuhan, China: a time-series study using a distributed lag non-linear model. Int J Environ Res Public Health 13:1–13. https://doi.org/10.3390/ijerph13070722

Zhang Y, Sun L (2019) Spatial-temporal impacts of urban land use land cover on land surface temperature: case studies of two Canadian urban areas. Int J Appl Earth Obs Geoinf 75:171–181. https://doi.org/10.1016/j.jag.2018.10.005

Zhou D, Xiao J, Bonafoni S et al (2018) Satellite remote sensing of surface urban heat islands: progress, challenges, and perspectives. Remote Sens 11:48. https://doi.org/10.3390/rs11010048

Zhou X, Chen H (2018) Impact of urbanization-related land use land cover changes and urban morphology changes on the urban heat island phenomenon. Sci Total Environ 635:1467–1476. https://doi.org/10.1016/j.scitotenv.2018.04.091